Impact of melting heat transfer in the time-dependent squeezing nanofluid flow containing carbon nanotubes in a Darcy-Forchheimer porous media with Cattaneo-Christov heat flux

Muhammad Ramzan[1,2], **Nomana Abid**[1], **Dianchen Lu**[3] **and Iskander Tlili**[4,5]

[1] Department of Computer Science, Bahria University, 44000, Islamabad, Pakistan
[2] Department of Mechanical Engineering, Sejong University, Seoul 143-747, Republic of Korea
[3] Department of Mathematics, Faculty of Science, Jiangsu University, Zhenjiang 212013, China
[4] Department for Management of Science and Technology Development, Ton Duc Thang University, Ho Chi Minh City, Vietnam
[5] Faculty of Applied Sciences, Ton Duc Thang University, Ho Chi Minh City, Vietnam

E-mail: iskander.tlili@tdtu.edu.vn

CrossMark

Abstract

This study aims to investigate the time-dependent squeezing of nanofluid flow, comprising carbon nanotubes of dual nature, e.g. single-walled carbon nanotubes, and multi-walled carbon nanotubes, between two parallel disks. Numerical simulations of the proposed novel model are conducted, accompanied by Cattaneo-Christov heat flux in a Darcy-Forchheimer permeable media. Additional impacts of homogeneous–heterogeneous reactions are also noted, including melting heat. A relevant transformation procedure is implemented for the transition of partial differential equations to the ordinary variety. A computer software-based MATLAB function, bvp4c, is implemented to handle the envisioned mathematical model. Sketches portraying impacts on radial velocity, temperature, and concentration of the included parameters are given, and deliberated upon. Skin friction coefficient and local Nusselt number are evaluated via graphical illustrations. It is observed that the local inertia coefficient has an opposite impact on radial velocity and temperature field. It is further perceived that melting and radiation parameters demonstrate a retarding effect on temperature profile.

(Some figures may appear in colour only in the online journal)

Nomenclature

Acronyms	Description		Symbols	Description
MWCNTs	Multi-walled carbon nanotubes		$b(t)$	Strength of magnetic field
MHD	Magnetohydrodynamics		c	Dimensional constant
SWCNTs	Single-walled carbon nanotubes		C_p	Capacity of specific heat
			c_s	Heat capacity of solid surface

$(C_p)_{nf}$	Specific heat capacity of nanofluid	ρ_c	Density of carbon nanotubes
D_m, D_n	Diffusion coefficients	$f(\chi)$	Axial velocity (dimensionless velocity)
$(C_p)_f$	Specific heat capacity of fluid	$H(\chi), G(\chi)$	Dimensionless concentrations
F^*	Forchheimer parameter	k_f	Base fluid (water) thermal conductivity
Ha	Hartmann number	μ	dynamic viscosity
k_c	Thermal conductivity of carbon nanotubes	μ_{nf}	Nanofluid dynamic viscosity
K^*	Permeability of spongy media	ρ_f	Density of fluid
k_1	Homogeneous reaction parameter	ν_{nf}	Nanofluid kinematic viscosity
k_2	Heterogeneous reaction parameter	ϕ	Volume fraction of nanoparticles
L	Latent heat	ν	Kinematic viscosity
m, n, K_i, K_j	Concentrations of chemical species	k^*	Mean absorption coefficient
F	Local inertia coefficient	λ	Porosity parameter
k	Thermal conductivity	*Subscripts*	*Description*
m^*, n^*	Chemical species	0	For solid
Me	Melting heat coefficient	1	For homogeneous
P	Pressure	2	For heterogeneous
q_{rd}	Radiative heat flux	c	Carbon nanotubes
Pr	Prandtl number	f	Fluid
R_d	Thermal radiation coefficient	H	For upper disk
Re_L	Local squeezed Reynolds number	L	For local
Re	Reynolds parameter	M	For lower disk
Sc	Schmidt parameter	nf	Nanofluid
Sq	Squeeze parameter	p	Constant pressure
T	Temperature	rd	Radiative
T_0	Temperature of solid	s	Solid surface
T_H	Temperature at upper disk		
T_M	Surface temperature		
(U^*, W^*)	Components of velocities		
K	Kelvin		
W	Watt		
Greek symbols	*Description*		
χ	Similarity transformation variable		
$\theta(\chi)$	Dimensionless temperature		
$f'(\chi)$	Radial velocity (dimensionless velocity)		
k_c	Carbon nanotubes thermal conductivity		
μ_f	fluid dynamic viscosity		
k_{nf}	Thermal conductivity of nanofluid		
ρ	Density		
ρ_{nf}	Nanofluid density		
σ_{nf}	Nanofluid electrical conductivity		
ν_f	Kinematic viscosity of the fluid		
σ^*	Stefan Boltzmann constant		
γ	Thermal relaxation coefficient		
θ_w	Temperature ratio parameter		

Introduction

A carbon nanotube is a large, stretched, thin, and tube-shaped molecule of pure carbon of around 1 to 3 nanometers (1 to 3 billionth of a meter) in breadth (diameter), and 100 to 1000 s of nanometers in length. Iijima [1] introduced the theory of carbon nanotubes at the end of the 20th century, when he discovered some potential applications of CNTs for solar cells, radar-absorbing coating, gas storage, composites, semiconductor devices, ultra-capacitors, etc [2]. CNTs are classified as SWCNTs and MWCNTs. A SWCNT has a regular straw shape with only one layer. A MWCNT is a set of nested SWCNTs of increasing diameters. Din and Khan [3] studied the squeezing flow of Casson fluid with non-linear thermal radiation between parallel disks. Haq *et al* [4] examined MHD nanofluid squeezed flow based on water with CNTs between 2-parallel disks, and concluded that temperature and velocity profiles increase with high nanoparticle volume fraction. Melting heat in the radiative flow of CNTs with homogeneous–heterogeneous reactions was scrutinized

by Hayat *et al* [5]. They found that the Nusselt number increases for large values of nanoparticle volume fraction.

Recently, squeezed flow between two parallel disks has garnered a great deal of attention, with its vast number of potential applications in technological and industrial systems. Many devices such as stirring pistons in engines, hydraulic brakes, and chocolate filler are based on the flow principle between squeezing regions. Stefan [6] proposed the idea of squeezing flow in 1874. Since then, many researchers have explored the problems associated with squeezing flow. The theoretical investigation regarding squeezing flow between parallel disks is presented by Leider and Bird [7]. Qayyum *et al* [8] discussed time-dependent squeezing Jeffery fluid flow between two parallel disks. Hayat *et al* [9] discussed squeezed nanofluid flow-based CNTs, and the impact of thermal radiations on Darcy-Forchheimer spongy media. They posited that an augmentation in nanoparticle volume fraction causes a reduction in both the velocity and the temperature of the fluid. Hashmi *et al* [10] investigated the analytical simulations for squeezing nanofluid flow amidst parallel disks. It should be noted that these studies are discuss the use of two parallel disks, but do not refer to Cattaneo-Christov heat flux.

The Fourier law of heat conduction has been a criterion benchmark in many practical industries for estimating the behavior of heat transmission. Nevertheless, because of the parabolic-heat equation due to an initial disorder, this system suffers a great deal. Cattaneo [11] tackled this drawback of the Fourier model via the addition of thermal time relaxation. This modification has created a hyperbolic heat equation for the temperature field. Also, within finite speeds, heat transmission is permitted to circulate through thermal waves. Tibullo and Zampoli [12] have worked on innumerable practicable applications i.e. to nanofluid flow, applying the Cattaneo-Christov heat conduction model. Christov [13] posited a modification of the Maxwell-Cattaneo model, which is known as the Cattaneo-Christov thermal flux model. Radiative nanofluid flow with the Cattaneo-Christov heat flux model between parallel disks is studied by Dogonchi *et al* [14]. Lu *et al* [15] discussed the mathematical model of unsteady fluid flow containing SWCNTs and MWCNTs under conditions of Cattaneo-Christov heat flux, and homogeneous–heterogeneous reactions between two parallel disks, and determined that temperature rises with an increasing thermal relaxation parameter. Zubair *et al* [16] discussed the 3D Darcy-Forchheimer squeezing nanofluid flow with Cattaneo-Christov heat flux, using four distinct types of nanoparticles, via the analysis of entropy generation.

Henry Darcy [17] determined the fluid flow over a permeable surface, based on the outcomes of water flow experiments over cribs of sand, and hydro-geology. He defined his idea of fluid flow over a spongy media in 1856. Due to its limitations of small velocity with weaker permeability, Philipps Forchheimer [18] modified the momentum equation by velocity square v^2 within Darcian velocity. This became known as the Forchheimer term, as designated by Muskat [19]. Nasir *et al* [20] scrutinized the radiative 3D

Darcy-Forchheimer flow of carbon nanotubes past a stretchable rotating disk. They posited that fluid velocity falls with an upsurge in inertia and porosity parameters. Jha and Kaurangini [21] presented analytic solutions for Darcy-Forchheimer-based spongy media relations. Kaladhar [22] discussed mixed convection flow with dual stratification effects within a Darcy-Forchheimer medium, finding that velocity is reduced for higher estimates of Darcy-Forchheimer number. A numerical solution for a second law analysis of ferrofluid within a spongy semi annulus is investigated by Sheikholeslami *et al* [23]. Alamri *et al* [24] proposed the model of a radiative plane Poiseuille flow of nanofluid, using slip conditions past a porous medium. Some recent investigations discussing porous media are referenced in [25–28], among many others.

Based on the above discussion, it can be noted that there is as yet no study in which the influences of Cattaneo-Christov heat flux with carbon nanotubes in a Darcy-Forchheimer porous media are examined between two parallel disks. Comparatively little research has been conducted in the area of carbon nanotubes to date. For this reason, this paper aims to examine melting heat transfer effects in carbon nanotubes- (SWCNTs and MWCNTs) based nanofluid unsteady flow, in a non-linear Darcy-Forchheimer permeable media, between two parallel disks, with Cattaneo-Christov heat flux and homogeneous–heterogeneous reactions. The impact of prominent parameters on surface drag force, and Nusselt number, are portrayed via graphic illustrations. The numerical solution of the present work is obtained by adopting the Finite difference method, this being the default in the bvp4c built-in function of the MATLAB scheme. The layout of this paper consists of: Section one – introduction. Section two is devoted to mathematical modeling, with all required equations, having employed the boundary layer theory to partial differential equations. Section three is a detailed elaboration of the numerical methods applied to the problem. Section four covers results and discussion. The paper concludes with Final remarks and summing up.

Mathematical modeling

Consider an incompressible, time-dependent 2D MHD nanofluid flow, containing CNTs within a Darcy-Forchheimer spongy media under conditions of non-linear thermal radiation and melting heat transfer, between two infinite parallel disks of length

$$Z = x(t) = h\sqrt{1 - ct}, \qquad (1)$$

with applied magnetic strength $b(t) = \frac{b_0}{\sqrt{1 - ct}}$ which is normal to the disks (figure 1). Here, SWCNTs and MWCNTs, along with water (base fluid), are considered. Moreover, the upper disk $Z = x(t)$ moves up and down with a velocity $\frac{d}{dt}(Z)$ from the fixed and porous lower disk $Z = 0$. The induced magnetic field is neglected here, because we are using a small Reynolds number. We also consider the cylindrical coordinate system
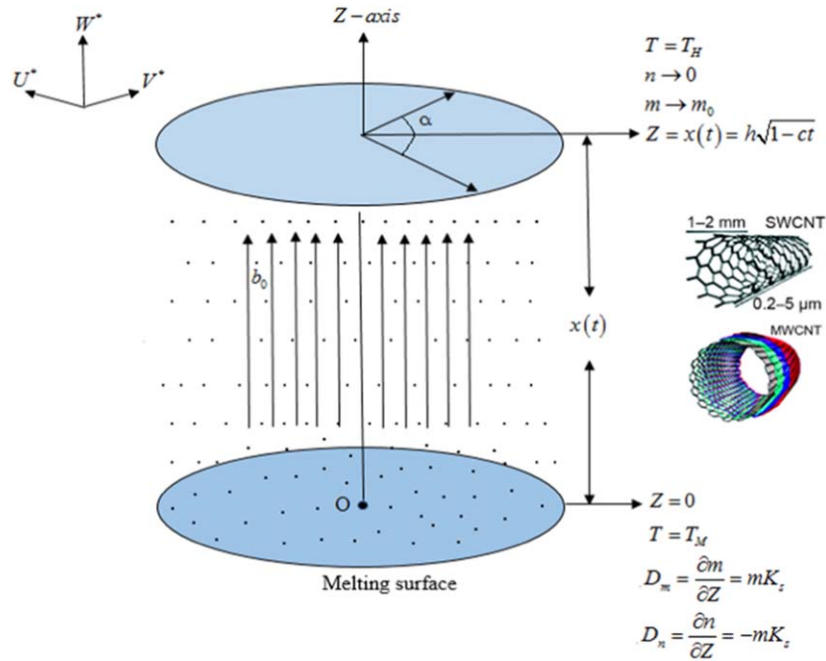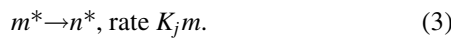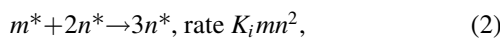
Figure 1. Fluid geometry.

(R, α, Z). The velocity component V vanishes identically due to rotational flow symmetry $\left(\frac{\partial}{\partial \alpha} = 0\right)$.

We assume a model, designed by Chaudhary and Merkin [29] for homogeneous–heterogeneous chemical reactions defined as:

$$m^* + 2n^* \rightarrow 3n^*, \text{ rate } K_i mn^2, \tag{2}$$

$$m^* \rightarrow n^*, \text{ rate } K_j m. \tag{3}$$

These reactions are presumed to be isothermal. The governing system with boundary layer equations are represented as:

$$\frac{\partial U^*}{\partial R} + \frac{U^*}{R} + \frac{\partial W^*}{\partial Z} = 0, \tag{4}$$

$$\frac{\partial U^*}{\partial t} + U\frac{\partial U^*}{\partial R} + W\frac{\partial U^*}{\partial Z} = -\frac{1}{\rho_{\text{nf}}}\frac{\partial P}{\partial R} + \frac{\mu_{\text{nf}}}{\rho_{\text{nf}}}\left(\frac{\partial^2 U^*}{\partial R^2}\right.$$
$$\left. + \frac{1}{R}\frac{\partial U^*}{\partial R} - \frac{U^*}{R^2} + \frac{\partial^2 U^*}{\partial Z^2}\right) - \frac{\sigma_{\text{f}}}{\rho_{\text{nf}}}b^2(t)U^*$$
$$- \frac{\nu_{\text{nf}} U^*}{K} - F^* U^{*2}, \tag{5}$$

$$\frac{\partial W^*}{\partial t} + U\frac{\partial W^*}{\partial R} + W\frac{\partial W^*}{\partial Z} = -\frac{1}{\rho_{\text{nf}}}\frac{\partial P}{\partial Z} + \frac{\mu_{\text{nf}}}{\rho_{\text{nf}}}\left(\frac{\partial^2 W^*}{\partial R^2}\right.$$
$$\left. + \frac{1}{R}\frac{\partial W^*}{\partial R} + \frac{\partial^2 W^*}{\partial Z^2}\right) - \frac{\nu_{\text{nf}} W^*}{K} - F^* W^{*2}, \tag{6}$$

$$\frac{\partial T}{\partial t} + U^*\frac{\partial T}{\partial R} + W^*\frac{\partial T}{\partial Z}$$
$$+ \varepsilon\begin{pmatrix} \frac{\partial^2 T}{\partial t^2} + \frac{\partial U^*}{\partial t}\frac{\partial T}{\partial R} + 2U^*\frac{\partial^2 T}{\partial t\partial R} + 2W^*\frac{\partial^2 T}{\partial t\partial Z} \\ + \frac{\partial W^*}{\partial t}\frac{\partial T}{\partial Z} + U^*\frac{\partial U^*}{\partial R}\frac{\partial T}{\partial R} + W^*\frac{\partial W^*}{\partial Z}\frac{\partial T}{\partial Z} + U^*\frac{\partial W^*}{\partial R}\frac{\partial T}{\partial Z} \\ + W^*\frac{\partial U^*}{\partial Z}\frac{\partial T}{\partial R} + 2U^*W^*\frac{\partial^2 T}{\partial R\partial Z} + U^{*2}\frac{\partial^2 T}{\partial R^2} + W^{*2}\frac{\partial^2 T}{\partial Z^2} \end{pmatrix}$$
$$= -\frac{k_{\text{nf}}}{(\rho C_p)_{\text{nf}}}\left(\frac{\partial^2 T}{\partial R^2} + \frac{1}{R}\frac{\partial T}{\partial R} + \frac{\partial^2 T}{\partial Z^2}\right) - \frac{1}{(\rho C_p)_{\text{nf}}}\frac{\partial q_{\text{rd}}}{\partial Z}, \tag{7}$$

$$\frac{\partial m}{\partial t} + U^*\frac{\partial m}{\partial R} + W^*\frac{\partial m}{\partial Z} = D_m\left(\frac{\partial^2 m}{\partial R^2} + \frac{1}{R}\frac{\partial m}{\partial R} + \frac{\partial^2 m}{\partial Z^2}\right)$$
$$- K_i mn^2, \tag{8}$$

$$\frac{\partial n}{\partial t} + U^*\frac{\partial n}{\partial R} + W^*\frac{\partial n}{\partial Z} = D_n\left(\frac{\partial^2 n}{\partial R^2} + \frac{1}{R}\frac{\partial n}{\partial R} + \frac{\partial^2 n}{\partial Z^2}\right)$$
$$+ K_i mn^2. \tag{9}$$

With boundary conditions

$$U^* = 0, \ W^* = \frac{d}{dt}(Z), \ T = T_H, \ m \rightarrow m_0, \ n \rightarrow 0,$$
$$\text{at } Z = x(t), \tag{10}$$

$$U^* = 0, \ k_{nf}\left(\frac{\partial T}{\partial Z}\right)_{Z=0} = \rho_{nf}(c_s(T_M - T_0) + L)W^*(R, 0),$$
$$T = T_M, \ D_m\frac{\partial m}{\partial Z} = mK_j, \ D_n\frac{\partial n}{\partial Z} = -mK_j, \ \text{at } Z = 0. \tag{11}$$

Table 1. Thermophysical characteristics of base fluid, SWCNTs and MWCNTs [30].

Thermophysical traits	$C_p\left(\dfrac{J}{kgK}\right)$	$\rho\left(\dfrac{kg}{m^3}\right)$	$k\left(\dfrac{W}{mK}\right)$
Water (base fluid)	4179.00	997.100	0.613 00
Nanoparticles (SWCNTs)	425	2600	6600
Nanoparticles (MWCNTs)	796	1600	3000

Mathematically, thermophysical properties are shown as:

$$\mu_{nf} = \frac{\mu_f}{(1-\phi)^{2.5}}, \quad \nu_{nf} = \frac{\mu_{nf}}{\rho_{nf}}, \quad \alpha_{nf} = \frac{k_{nf}}{(\rho C_p)_{nf}},$$

$$\nu_f = \frac{\mu_f}{\rho_f}, \quad \frac{k_{nf}}{k_f} = \frac{(1-\phi) + 2\phi\dfrac{k_C}{k_C - k_f}\ln\dfrac{k_C + k_f}{2k_f}}{(1-\phi) + 2\phi\dfrac{k_C}{k_C - k_f}\ln\dfrac{k_C + k_f}{2k_f}},$$

$$\rho_{nf} = (1-\phi)\rho_f + \phi\rho_C, \quad (\rho C_p)_{nf} = (1-\phi)(\rho C_p)_f + \phi(\rho C_p)_C. \tag{12}$$

The thermophysical features of water and CNTs are appended in table 1.

From equation (7), by utilizing the Roseland thermal radiation approximation [31], we obtain the value of q_{rd} as:

$$q_{rd} = -\frac{4\sigma^*}{3k^*}\frac{\partial T^4}{\partial Z} = -\frac{16\sigma^*}{3k^*}T^3\frac{\partial T}{\partial Z}, \tag{13}$$

with

$$T = T_M[1 + (\theta_w - 1)\theta]. \tag{14}$$

Similarity transformation

Similarity transformations are defined as:

$$U^* = \frac{cR}{2(1-ct)}f'(\chi), \quad W^* = -\frac{ch}{(1-ct)^{\frac{1}{2}}}f(\chi),$$

$$m = m_0 H(\chi), \quad n = m_0 G(\chi), \quad b(t) = \frac{b_0}{(1-ct)^{\frac{1}{2}}},$$

$$\chi = \frac{Z}{h(1-ct)^{\frac{1}{2}}}, \quad \theta = \frac{T - T_M}{T_H - T_M}. \tag{15}$$

By means of the above transformation, equation (4) is satisfied, and equations (5)–(9) are transformed into:

$$\frac{1}{(1-\phi)^{2.5}}f''''(\chi) - \left[(1-\phi) + \phi\frac{\rho_c}{\rho_f}\right]$$

$$\times\left[\begin{array}{l}3Sqf''(\chi) + Sq\chi f'''(\chi)\\ -2Sqf(\chi)f'''(\chi) + \mathrm{Re}\, Ff'(\chi)f''(\chi)\end{array}\right]$$

$$-\left[\frac{\lambda\,\mathrm{Re}}{(1-\phi)^{2.5}} + Ha\right]f''(\chi) = 0, \tag{16}$$

$$\frac{k_{nf}}{k_f}\{[1 + R_d(1 + (\theta_w - 1)\theta)^3]\theta'\}'$$

$$+ SqPr\left[(1-\phi) + \phi\frac{(\rho C_p)_c}{(\rho C_p)_f}\right]$$

$$\left\{(2f(\chi) - \chi)\theta'(\chi) - \gamma\left[\begin{array}{l}\begin{pmatrix}\chi^2 - 4\chi f(\chi)\\ +4f^2(\chi)\end{pmatrix}\theta''(\chi)\\ +\begin{pmatrix}4f(\chi)f'(\chi) + 3\chi\\ -2\chi f'(\chi) - 6f(\chi)\end{pmatrix}\theta'(\chi)\end{array}\right]\right\}$$

$$= 0, \tag{17}$$

$$\frac{1}{Sc}H''(\chi) + f(\chi)H'(\chi) - \frac{\chi}{2}H'(\chi) - k_1 H(\chi)G^2(\chi) = 0, \tag{18}$$

$$\frac{\delta}{Sc}G''(\chi) + f(\chi)G'(\chi) - \frac{\chi}{2}G'(\chi) + k_1 H(\chi)G^2(\chi) = 0, \tag{19}$$

with

$$\delta = \frac{D_n}{D_m}. \tag{20}$$

Based on equations (2) and (3), chemical species m^* and n^* cannot be analogous, but both can be identical in magnitude, provided $\delta = 1$. Thus, from equation (20), presuming that D_n and D_m are identical (i.e., $\delta = 1$), we obtain

$$H(\chi) + G(\chi) = 1, \tag{21}$$

using the above property, equations (18) and (19) become

$$\frac{1}{Sc}H''(\chi) + f(\chi)H'(\chi) - \frac{\chi}{2}H'(\chi)$$

$$- k_1 H(\chi)[1 - H(\chi)]^2 = 0, \tag{22}$$

and the boundary Equations (10) and (11) become

$$f'(0) = 0, \quad \theta(0) = 0, \quad \frac{k_{nf}}{k_f}M_e\theta'(0) + PrRe\left[(1-\phi)\right.$$

$$\left.+\phi\frac{\rho_c}{\rho_f}\right]f(0) = 0, \quad H'(0) = k_2 H(0), \text{ at } \chi = 0, \tag{23}$$

$$f(1) = \frac{1}{2}, \quad f'(1) = 0, \quad \theta(1) = 1, \quad H(1) \to 1, \text{ at } \chi = 1. \tag{24}$$

Based on equation (23), M_e is the melting heat coefficient as:

$$M_e = \left[\frac{c_f(T_H - T_M)}{L + c_s(T_M - T_0)}\right], \tag{25}$$

which is the amalgamation of two numbers, $c_f(T_H - T_M)/L$, and $c_s(T_M - T_0)/L$, known as Stefan numbers, for solid and liquid states. In the above equations, non-dimensional coefficients are defined as:

$$Sq = \frac{ch^2}{2\nu_f}, \quad Ha = \left(\frac{\sigma_f b_0{}^2 h^2}{\mu_f}\right)^{\frac{1}{2}}, \quad Pr = \frac{\mu_f(\rho C_p)_c}{\rho_f k_f},$$

$$Re = \frac{ch^2}{\nu_f}, \quad F = F^* R = \frac{C_b R}{(K^*)^{\frac{1}{2}}}, \quad \lambda = \frac{\nu_f}{cK^*},$$

$$R_d = \frac{16\sigma^* T_M{}^3}{3k^* k_f}, \quad k_1 = \frac{K_i A_0{}^2(1 - ct)}{c},$$

$$\gamma = \frac{\varepsilon c}{2(1 - ct)}, \quad Sc = \frac{ch^2}{D_m}, \quad k_2 = \frac{K_j h(1 - ct)^{\frac{1}{2}}}{D_m}. \quad (26)$$

Surface drag force and rate of heat flux are classified by:

$$C_{fr} = \frac{\mu_{\mathrm{nf}}\left(\dfrac{\partial U^*}{\partial Z} + \dfrac{\partial W^*}{\partial R}\right)_{Z=x(t)}}{\rho_{\mathrm{f}}\left(-\dfrac{ch}{2\sqrt{1 - ct}}\right)^2},$$

$$Nu = \frac{k_{\mathrm{nf}} h}{k_{\mathrm{f}}(T_H - T_M)}\left[(q_r)_w - \left(\frac{\partial T}{\partial Z}\right)_{Z=x(t)}\right], \quad (27)$$

using equation (15), we get

$$\frac{h^2}{R^2} Re_L C_{fr} = \left[\frac{1}{(1 - \phi)^{2.5}\left[(1 - \phi) + \phi\dfrac{\rho_c}{\rho_{\mathrm{f}}}\right]}\right] f''(1),$$

$$\sqrt{1 - ct}\, Nu = -\left[\frac{k_{\mathrm{nf}}}{k_{\mathrm{f}}}\right.$$
$$\left. + R_d(1 + (\theta_W - 1)\theta(1))^3\right]\theta'(1), \quad (28)$$

where

$$Re_L = \frac{\rho_f R c h\sqrt{1 - ct}}{2\mu_{\mathrm{f}}}. \quad (29)$$

Solution methodology

For non-linear systems of ODEs (16), (17), and (22), with boundary conditions (23) and (24), we employ the finite difference default method of the bvp4c built-in function of the MATLAB scheme, which is fourth order accurate, and a grid size of 0.01 is taken with the tolerance 10^{-7}. Using the following numerical code, we obtain first order ODEs as:

$$y_{(1)} = f(\chi), \quad y_{(2)} = f'(\chi), \quad y_{(3)} = f''(\chi),$$
$$y_{(4)} = f''(\chi),$$

$$f''''(\chi) = [y'_{(4)}] = yy_{(1)} = (1 - \phi)^{2.5}\left\{(1 - \phi)\right.$$
$$\left. + \phi\frac{\rho_c}{\rho_f}\right\}\left\{\begin{array}{l} 3Sqy_{(3)} + Sq\chi y_{(4)} \\ -2Sqy_{(1)}y_{(4)} + ReFy_{(2)}y_{(3)} \end{array}\right\}$$
$$+ \{\lambda Re + Ha(1 - \phi)^{2.5}\}y_{(3)}, \quad (30)$$

$$y_{(5)} = \theta(\eta), \quad y_{(6)} = \theta'(\chi),$$
$$\theta''(\chi) = [y'_{(6)}] = yy_{(2)}$$

$$= \left(\begin{array}{c} -SqPr\left\{(1 - \phi) + \phi\dfrac{(\rho C_p)_c}{(\rho C_p)_f}\right\}\left[\begin{array}{c} (2y_{(1)} - \chi)y_{(6)} - \\ \gamma\left\{\begin{array}{l} 4y_{(1)}y_{(2)} + 3\chi \\ -2\chi y_{(2)} - 6y_{(1)} \end{array}\right\}y_{(6)} \end{array}\right] \\[4mm] \dfrac{-\dfrac{k_{nf}}{k_f}3R_d\{1 + (\theta_w - 1)y_{(5)}\}^2(y_{(6)})^2}{SqPr\gamma\left\{(1 - \phi) + \phi\dfrac{(\rho C_p)_c}{(\rho C_p)_f}\right\}\left(\begin{array}{c} \chi^2 - 4\chi y_{(1)} \\ +4(y_{(1)})^2 \end{array}\right)} \\[6mm] +\dfrac{k_{nf}}{k_f}[1 + R_d\{1 + (\theta_w - 1)y_{(5)}\}^3] \end{array}\right);$$

$$y_{(7)} = H(\chi), \quad y_{(8)} = H'(\chi),$$
$$(31)$$

$$H''(\chi) = [y'_{(8)}] = yy_{(3)} = Sc\left[\frac{\chi}{2}y_{(8)} - y_{(1)}y_{(8)}\right.$$
$$\left. + k_1 y_{(7)}[1 - y_{(7)}]^2\right]. \quad (32)$$

With the boundary conditions

$$y_{(2)}(0) = 0, \ y_{(5)}(0) = 0, \ \frac{k_{nf}}{k_f}M_e y_{(6)}(0) + \left\{(1 - \phi)\right.$$
$$\left. + \phi\frac{\rho_c}{\rho_f}\right\}PrRe y_{(1)}(0) = 0, \ y_{(8)}(0) = k_2 y_{(7)}(0), \quad (33)$$

$$y_1(\infty) - \frac{1}{2}; \ y_2(\infty); \ y_5(\infty) - 1; \ y_7(\infty) - 1. \quad (34)$$

Results and discussion

This segment examines the outcomes of dimensionless velocity $f'(\chi)$, temperature $\theta(\chi)$, and concentration fields $H(\chi)$ for numerous arising parameters, so as to reflect the behavior of fluid flow, and heat and mass transport. The subsequent discussion is presented for both SWCNTs and MWCNTs. Parameters used in this analysis are $Pr = 6.2$, $Re = 0.4$, $\lambda = 0.2$, $Ha = 0.5$, $M_e = 0.01$, $\gamma = 0.5$, $Sq = Sc = 1.0$, $k_1 = k_2 = 0.7$, $\phi = F = 0.1$, $R_d = 0.9$, $\theta_w = 1.1$. Figure 2(a) illustrates how positive and negative values of squeezed number S_q affect velocity $f'(\chi)$. The graph illustrates how, for both single and multi-walled CNTs, velocity profile $f'(\chi)$ increases with the contraction of disks, i.e., negative values, whereas for positive values where upper and lower plates are driven further apart, the opposite behavior can be observed. In the case of contraction $(S_q = -1, -2, -3...)$, the fluid is exposed to a squeezed force, which causes it to move with increased velocity. Hence, velocity is augmented. Nevertheless, for $S_q = 1, 2, 3...$ when both disks move away from each other, a gap is produced between the disks. The fluid moves in a reverse direction to fill this gap; thus, velocity reduces. In figure 2(b) effect of the S_q squeezing parameter is exhibited versus $\theta(\chi)$. In the case of the contraction
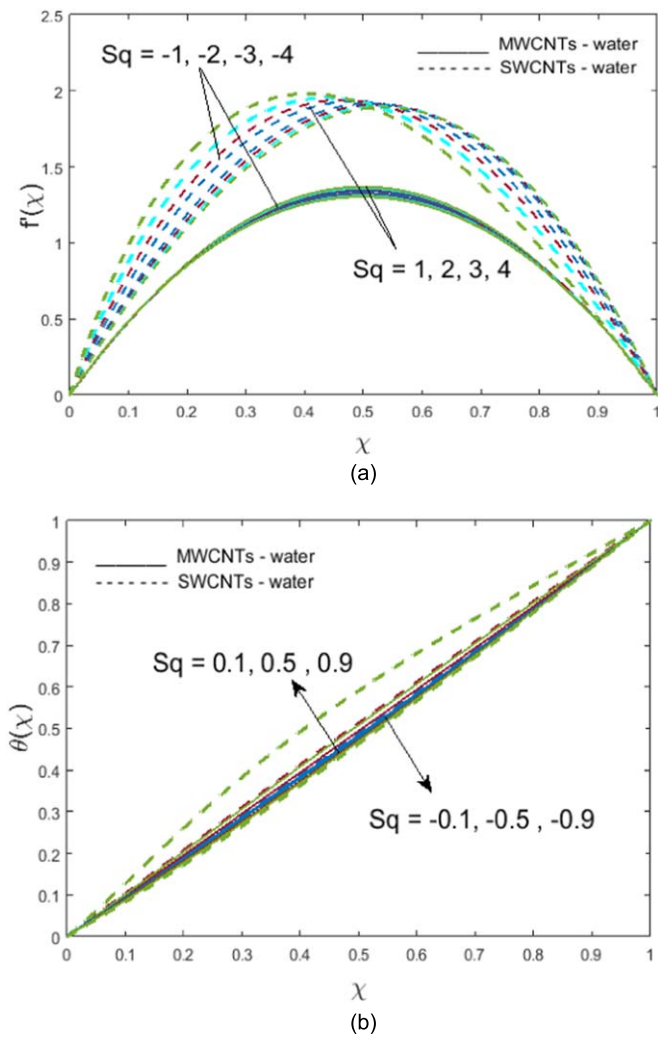
(a)

(b)

Figure 2. (a). Variations of squeezing parameter S_q on radial velocity $f'(\chi)$. (b). Variations of squeezing parameter S_q on temperature distribution $\theta(\chi)$.
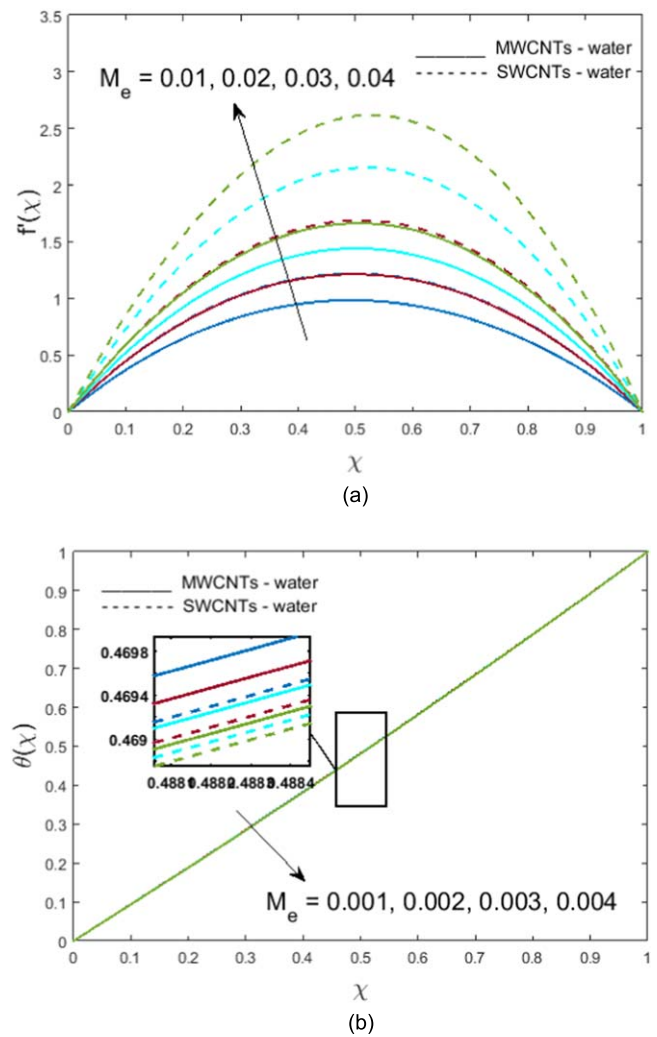

(a)

(b)

Figure 3. (a). Variations of melting parameter M_e on radial velocity $f'(\chi)$. (b). Variations of melting parameter M_e on temperature distribution $\theta(\chi)$.

of disks ($S_q = -1, -2, -3...$), the temperature profile $\theta(\chi)$ establishes diminishing behavior, whereas an opposite trend is seen when the disks are driven apart from each other i.e. $S_q = 1, 2, 3...$. This is because movement of fluid increases when disks are driving away from each other, thus the temperature increases. An inverse impact of the melting heat transfer parameter M_e can be observed in figures 3(a) and (b), for velocity $f'(\chi)$ and temperature $\theta(\chi)$ profiles, respectively. As the molecular motion enhances due to melting heat transit, owing to the fact that M_e leads to increased molecular motion from hot fluid toward cold surface, which in turn causes an increase in velocity. In contrast, with the temperature field, convective flow causes heat transfer to the melting surface more promptly, which results in decreasing temperature $\theta(\chi)$. Figures 4(a) and (b) depict the effect of the local inertia coefficient F on velocity $f'(\chi)$ and temperature $\theta(\chi)$ of fluid flow. It can be observed that local inertia coefficient F has an inverse influence on both fields. Here, velocity falls whereas temperature increases. As porous media cause resistance in a fluid flow, the

result is a reduction in dimensionless velocity $f'(\chi)$. Figure 5 illustrates the behavior of the temperature ratio parameter θ_w on fluid temperature. A retarding effect of θ_w on dimensionless temperature can be observed. The effects of porosity parameter λ on radial velocity are shown in figure 6, where velocity falls for higher values of λ. The porosity of spongy media causes high resistivity to fluid flow; hence, velocity declines. Figures 7(a) and (b) show the impact of the nanoparticle volume fraction parameter ϕ on the radial velocity $f'(\chi)$, and temperature $\theta(\chi)$ of the fluid. An increase in the quantity of nanoparticles in the base fluid (water) leads to a thickening of the fluid. Due to this, velocity reduces (figure 7(a)). On the other hand, in figure 7(b), for ordinary fluid (i.e., $\phi = 0$, in the absence of volume proportion) the temperature field is highest when the disks are driven further from each other (i.e., $S_q = 1, 2, 3...$), while augmentation of volume fraction ϕ causes a reduction in the temperature of the fluid. This is because the thermal conductivity of nanofluid increases by using a small concentration of nanoparticles, and when we increase the volume of nanoparticles,
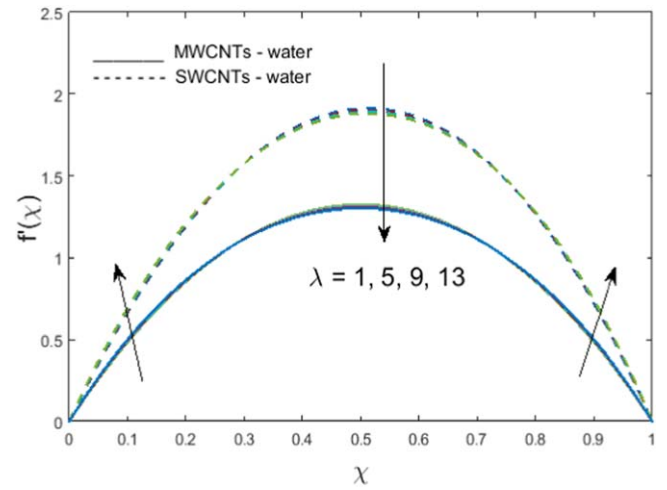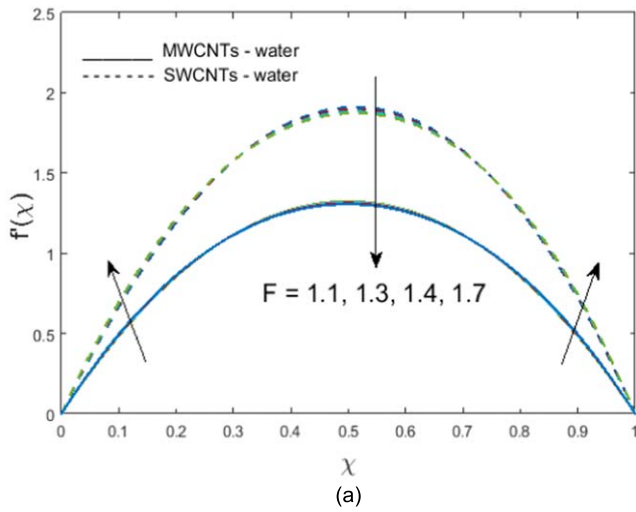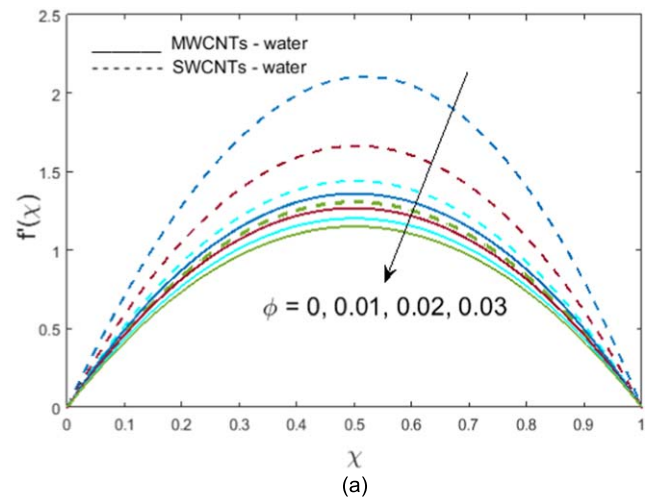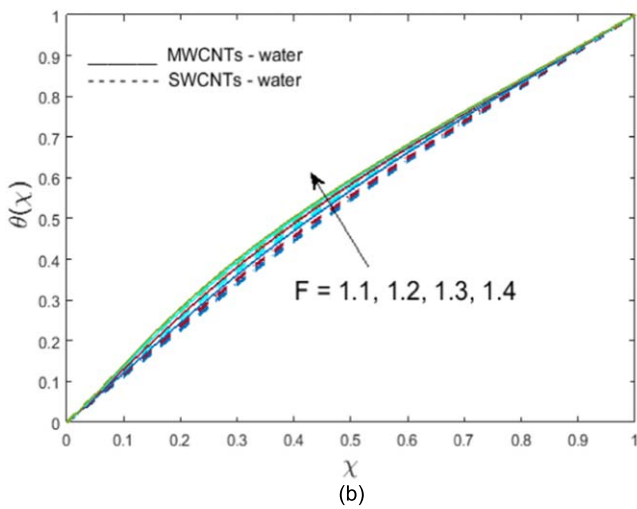
(a)

(b)

Figure 4. (a). Variations of local inertia coefficient F on radial velocity $f'(\chi)$. (b). Variations of local inertia coefficient F on temperature distribution $\theta(\chi)$.
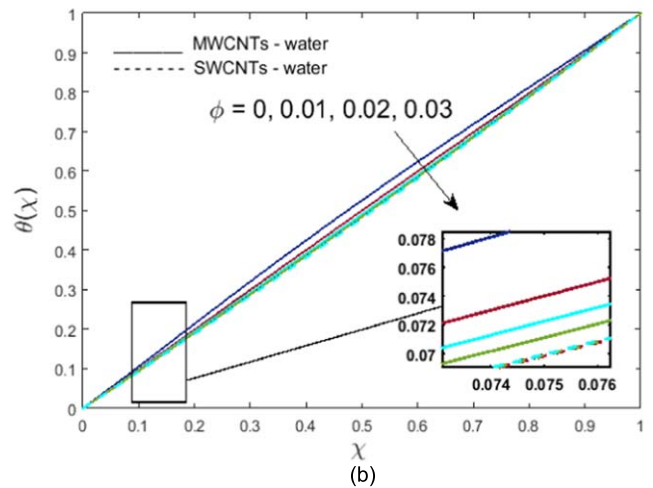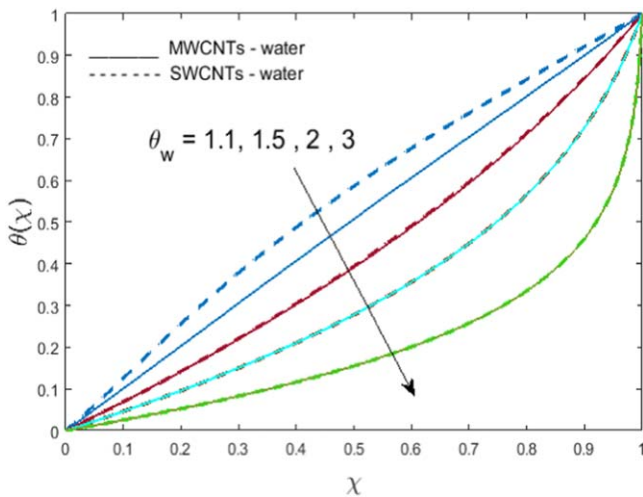

Figure 5. Variations of temperature ratio parameter θ_w on temperature distribution $\theta(\chi)$.

Figure 6. Variations of porosity parameter λ on radial velocity $f'(\chi)$.

(a)

(b)

Figure 7. (a). Variations of nanoparticle volume fraction ϕ on radial velocity $f'(\chi)$. (b). Variations of nanoparticle volume fraction ϕ on temperature distribution $\theta(\chi)$.
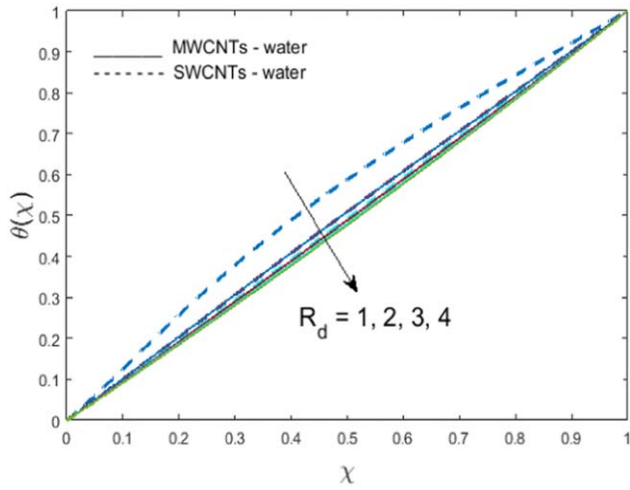
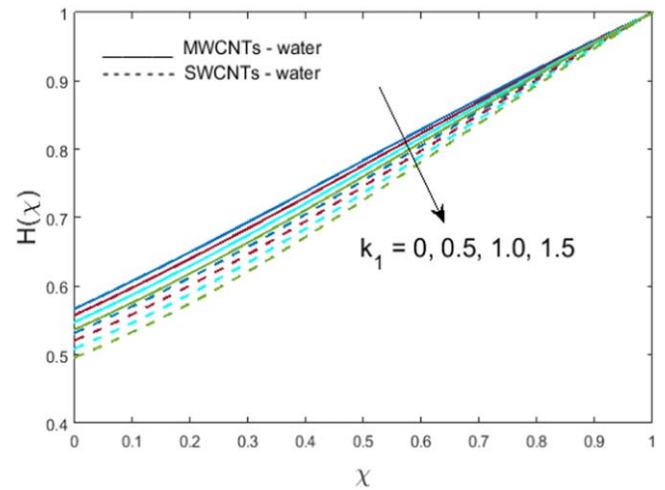**Figure 8.** Variations of radiation coefficient R_d on temperature distribution $\theta(\chi)$.

Figure 9. Variations of thermal relaxation parameter γ on temperature distribution $\theta(\chi)$.

Figure 10. Variations of homogeneous reaction Coefficient k_1 on concentration distribution $H(\chi)$.
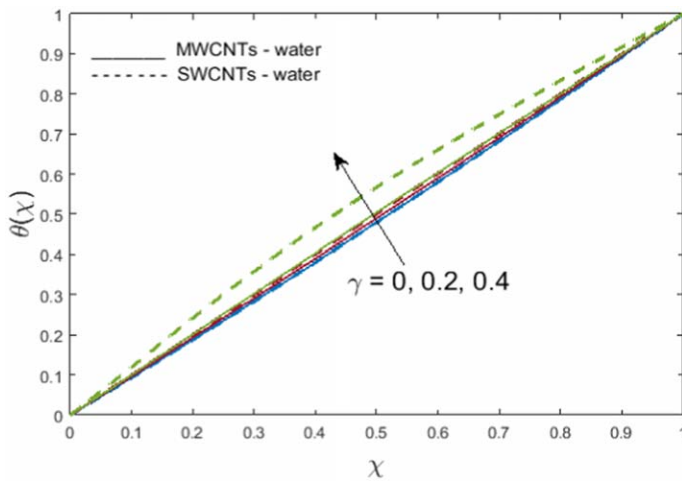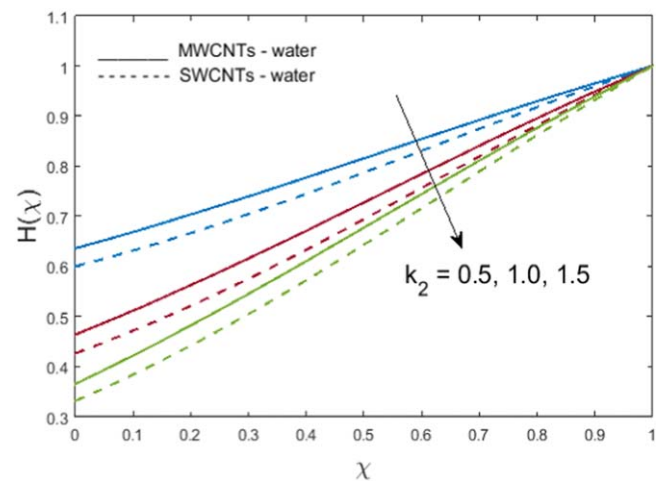

Figure 11. Variations of heterogeneous reaction coefficient k_2 on concentration distribution $H(\chi)$.

Figure 12. Variations of Schmidt number S_c on concentration distribution $H(\chi)$.

the thermal conductivity of the nanofluid decreases; hence, the temperature decreases. Figure 8 demonstrates the effects of the radiation parameter R_d on the temperature $\theta(\chi)$. The temperature drops for larger values of R_d. The transfer of energy to the fluid declines owing to higher estimates of R_d, thus decreasing the fluid temperature. In figure 9, the impact of the thermal relaxation time coefficient γ is shown. Higher values of γ cause an increment in dimensionless temperature $\theta(\chi)$ for both types of CNTs. Figure 10 indicates that concentration $H(\chi)$ decreases for higher values of k_1. The same outcome can be detected in figure 11 for k_2. It is therefore deduced that concentration eventually reduces as the reactants are used throughout homogeneous–heterogeneous reactions. The effects of Schmidt number Sc are portrayed in figure 12. The concentration profile is reduced for increasing values of Sc. As Sc is the ratio of momentum to mass diffusivity, greater Sc estimates indicate lower mass diffusivity, which causes a reduction in fluid concentration $H(\chi)$. In figure 13, a retardation effect of porosity
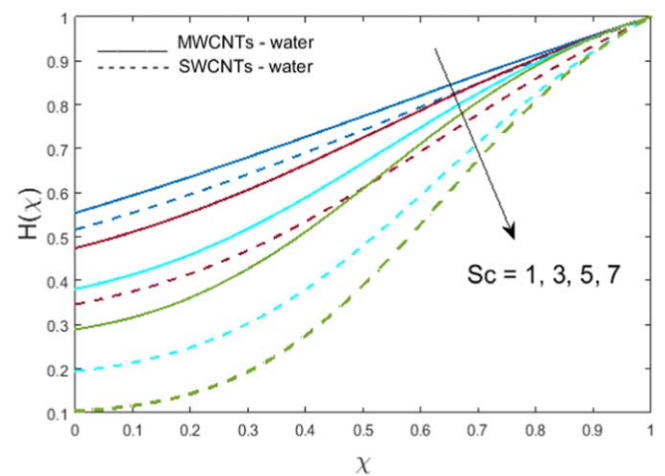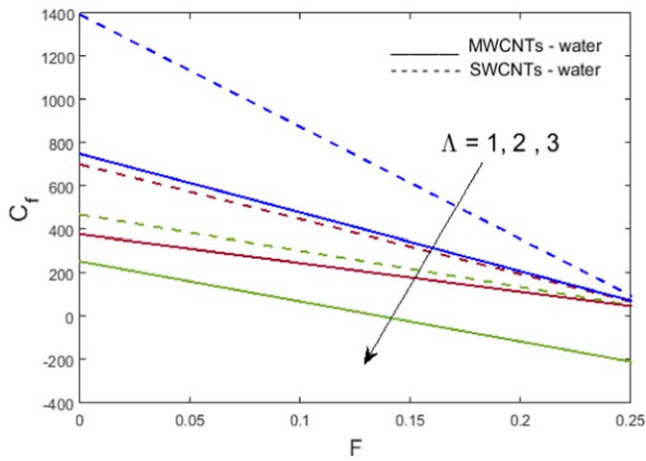
Figure 13. Variations of porosity parameter λ and local inertia parameter F on surface drag force.
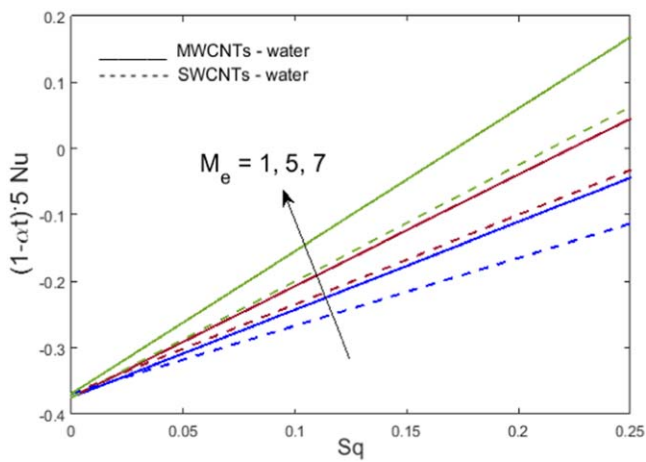

Figure 14. Variations of melting parameter M_e and squeezing parameter S_q on Nusselt number.
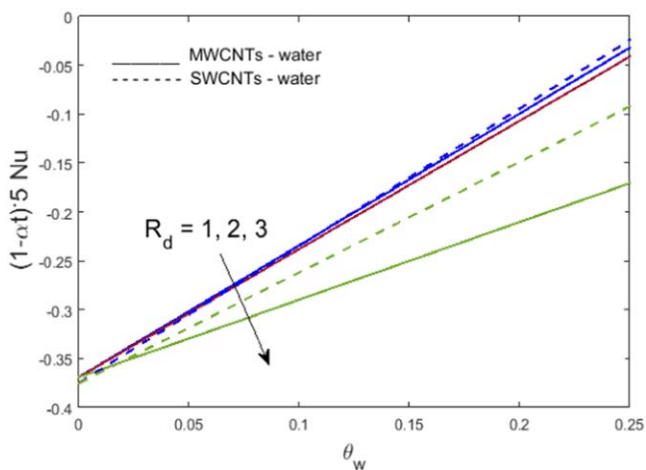

Figure 15. Variations of radiation parameter R_d and temperature ratio parameter θ_w on Nusselt number.

parameter λ on local inertia coefficient F can be observed for surface drag force. Influences of melting parameter M_e and squeezing parameter S_q on the rate of heat transfer are depicted

Table 2. Comparative results of surface drag force for distinct values of squeezing parameter and Hartmann number with Lu *et al* [15].

S_q	Ha	Lu *et al* [15]	Present results
0.5	0.0	−3.146 1941	−3.134 6178
	1.0	−3.194 0816	−3.183 3610
	2.0	−3.241 3602	−3.236 7145
−1.0	1.0	−2.759 6174	−2.747 1465
0.0		−3.049 6468	−3.031 1268
1.0		−3.338 1297	−3.327 8263

in figure 14. Here, it can be observed that augmentation in the melting coefficient M_e causes an increment in the rate of heat transfer. Since molecular motion increases with high melting heat transmission, hence the rate of heat is increased when we augment the melting parameter. Figure 15 illustrates the impact of radiation coefficient R_d and temperature ratio coefficient θ_w on the Nusselt number. The rate of heat transfer falls for larger estimates of R_d. This is because the energy from radiation phenomena is being used in the melting .process; thus, a significant decay in the Nusselt number can be seen.

Table 2 depicts the comparative estimates of surface drag force for various values of squeezing parameter and Hartmann number, with Lu *et al* [15] as limiting case. A remarkable resemblance is achieved in this regard.

Concluding remarks

In the presented model, 2D time-dependent magnetohydrodynamic squeezing nanofluid flow between two parallel disks with suspended carbon nanotubes is discussed. The analysis is performed under conditions of non-linear thermal radiation, amalgamated with melting heat, and homogeneous–heterogeneous reactions. Cattaneo-Christov heat flux is engaged in place of the conventional Fourier law of heat conduction. The proposed model is transformed into a non-linear form and processed by means of the default Finite difference method of the bvp4c built-in function of the MATLAB scheme. The key findings of the presented model are:

- The local inertia coefficient has an opposite impact on the radial velocity and temperature field.
- Porous media creates resistance in a fluid flow, resulting in a reduction in fluid velocity and an augmentation in the temperature of the fluid.
- The melting parameter has a retarding effect on temperature, whereas radial velocity increases.
- An increase in the radiation coefficient leads to a reduction in the temperature of the fluid.
- Radiative energy is being used in the melting process; consequently, the temperature of the fluid decreases.
- The porosity coefficient has a retarding influence on radial velocity and surface drag force.

Acknowledgments

This work is supported by Bahria University, Islamabad, Pakistan.

Competing interests statement

Authors have no conflict of interest regarding this publication.

References

[1] Iijima S 1991 Helical microtubules of graphitic carbon *Nature* **354** 56

[2] Endo M *et al* 2004 Applications of carbon nanotubes in the twenty-first century *Phil. Trans. R. Soc.* A **362** 1823

[3] Mohyud-Din S T and Khan S I 2016 Nonlinear radiation effects on squeezing flow of a Casson fluid between parallel disks *Aerosp. Sci. Technol.* **48** 186–92

[4] Haq R U, Hammouch Z and Khan W A 2016 Water-based squeezing flow in the presence of carbon nanotubes between two parallel disks *Therm. Sci.* **20** 1973–81

[5] Hayat T, Muhammad K, Muhammad T and Alsaedi A 2018 Melting heat in radiative flow of carbon nanotubes with homogeneous-heterogeneous reactions *Commun. Theor. Phys.* **69** 441

[6] Stefan M J 1874 'Versuch uber die scheinbare adhesion', Akademie Der Wissenschaften in Wien *Math. Natur.* **69** 713–21

[7] Leider P J and Bird R B 1974 Squeezing flow between parallel disks, I. Theoretical analysis *Ind. Eng. Chem. Fund.* **13** 336–41

[8] Qayyum A, Awais M, Alsaedi A and Hayat T 2012 Unsteady squeezing flow of Jeffrey fluid between two parallel disks *Chin. Phys. Lett.* **29** 034701

[9] Hayat T, Haider F, Muhammad T and Alsaedi A 2018 Darcy–Forchheimer squeezed flow of carbon nanotubes with thermal radiation *J. Phys. Chem. Solids* **120** 79–86

[10] Hashmi M M, Hayat T and Alsaedi A 2012 On the analytic solutions for squeezing flow of nanofluid between parallel disks *Nonlinear Anal. Model. Control* **17** 418–30

[11] Cattaneo C 1948 Sulla conduzione del calore *Atti Sem Mat Fis Univ Modena* **3** 83–101

[12] Tibullo V and Zampoli V 2011 A uniqueness result for the Cattaneo– Christov heat conduction model applied to incompressible fluids *Mech. Res. Commun.* **38** 77–9

[13] Christov C I 2009 On frame indifferent formulation of the Maxwell–Cattaneo model of finite-speed heat conduction *Mech. Res. Commun.* **36** 481–6

[14] Dogonchi A S, Chamkha A J, Seyyedi S M and Ganji D D 2018 Radiative nanofluid flow and heat transfer between parallel disks with penetrable and stretchable walls considering Cattaneo–Christov heat flux model *Heat Transf - Asian Res.* **47** 735–53

[15] Lu D, Li Z, Ramzan M, Shafee A and Chung J D 2019 Unsteady squeezing carbon nanotubes-based nano-liquid flow with Cattaneo–Christov heat flux and homogeneous–heterogeneous reactions *Appl. Nanosci.* **9** 169–78

[16] Zubair M, Shah Z, Islam S, Khan W and Dawar A 2019 Study of three-dimensional Darcy–Forchheimer squeezing nanofluid flow with Cattaneo–Christov heat flux based on four different types of nanoparticles through entropy generation analysis *Adv. Mech. Eng.* **11** 1–17

[17] Darcy H 1856 *Les Fontaines Publiques de la ville de Dijon: Exposition et Application* (Victor Dalmont)

[18] Forchheimer P 1901 Wasserbewegung durch boden *Z. Ver. Deutsch, Ing.* **45** 1782–8

[19] Muskat M 1938 The flow of homogeneous fluids through porous media *Soil Sci.* **46** 169

[20] Nasir S, vShah Z, Islam S, Khan W, Bonyah E, Ayaz M and Khan A 2019 Three dimensional Darcy-Forchheimer radiated flow of single and multiwall carbon nanotubes over a rotating stretchable disk with convective heat generation and absorption *AIP Adv.* **9** 035031

[21] Jha B K and Kaurangini M L 2011 Approximate analytical solutions for the nonlinear Brinkman-Forchheimer-extended Darcy flow model *Appl. Math.* **2** 1432–6

[22] Kaladhar K 2017 Double stratification effects on mixed convection flow of couple stress fluid in a non-Darcy porous medium with heat and mass fluxes *Comput. Appl. Math.* **36** 611–26

[23] Sheikholeslami M, Ellahi R, Shafee A and Li Z 2019 Numerical investigation for second law analysis of ferrofluid inside a porous semi annulus *Int. J. Numer. Method. H* **29** 1079–102

[24] Alamri S Z, Ellahi R, Shehzad N and Zeeshan A 2019 Convective radiative plane Poiseuille flow of nanofluid through porous medium with slip: an application of Stefan blowing *J. Mol. Liq.* **273** 292–304

[25] Sheikholeslami M 2019 New computational approach for exergy and entropy analysis of nanofluid under the impact of Lorentz force through a porous media *Comput. Method. Appl.* M **344** 319–33

[26] Li Z, Shafee A, Ramzan M, Rokni H B and Al-Mdallal Q M 2019 Simulation of natural convection of Fe_3O_4-water ferrofluid in a circular porous cavity in the presence of a magnetic field *Eur. Phys. J Plus.* **134** 77

[27] Bhatti M M, Zeeshan A, Ellahi R, Bég O A and Kadir A 2019 Effects of coagulation on the two-phase peristaltic pumping of magnetized Prandtl biofluid through an endoscopic annular geometry containing a porous medium *Chin. J. Phys.* **58** 222–34

[28] Li Z, Ramzan M, Shafee A, Saleem S, Al-Mdallal Q M and Chamkha A J 2019 Numerical approach for nanofluid transportation due to electric force in a porous enclosure *Microsyst. Technol.* **25** 2501–14

[29] Chaudhary M A and Merkin J H 1995 A simple isothermal model for homogeneous heterogeneous reactions in boundary-layer flow. I Equal diffusivities *Fluid Dyn. Res.* **16** 311

[30] Khan U, Ahmed N and Mohyud-Din S T 2017 Numerical investigation for three-dimensional squeezing flow of nanofluid in a rotating channel with lower stretching wall suspended by carbon nanotubes *Appl. Therm. Eng.* **113** 1107–17

[31] Rosseland S 1931 *Astrophysics and Nuclear-Theoretical Foundations* 41–4